INDIAN JOURNAL OF SCIENCE AND TECHNOLOGY

RESEARCH ARTICLE

Adaptive Sparsity through Hybrid Regularization for Effective Image Deblurring

S Pooja[1], S Mallikarjunaswamy[2]*, N Sharmila[3]

1 Research Scholar, Department of ECE, Research Scholar, Department of ECE, Bangalore, 560060, Karnataka, India
2 Associate Professor, Department of ECE, JSS Academy of Technical Education, Bangalore, 560060, Karnataka, India
3 Assistant Professor, Department of EEE, RNS Institute of Technology, Bangalore, 560060, Karnataka, India

OPEN ACCESS

Received: 17.04.2021
Accepted: 06.06.2021
Published: 16.07.2021

Citation: Pooja S, Mallikarjunaswamy S, Sharmila N (2021) Adaptive Sparsity through Hybrid Regularization for Effective Image Deblurring. Indian Journal of Science and Technology 14(24): 2051-2068. https://doi.org/10.17485/IJST/v14i24.604

* **Corresponding author**.

pruthvi.malli@gmail.com

Funding: None

Competing Interests: None

Copyright: © 2021 Pooja et al. This is an open access article distributed under the terms of the Creative Commons Attribution License, which permits unrestricted use, distribution, and reproduction in any medium, provided the original author and source are credited.

Published By Indian Society for Education and Environment (iSee)

ISSN
Print: 0974-6846
Electronic: 0974-5645

Abstract

Objectives: To develop image deblurring algorithm to effectively recover the original image from the captured blurry and noisy image. **Methods**: A novel image deblurring algorithm using adaptive priors is proposed. The adaptive priors vary the sparsity induced based on factors such as the type of blur affecting the image, image region, statistical parameters regarding the blur kernel and/or statistical predictions on the blur kernel. The proposed algorithm using adaptive priors improves the quality of the deblurred result, when compared with various recent image deblurring algorithms. **Finding:** the work contains a case study with regard to certain standard parameters. It is observed that proposed method is better in terms of frequency response, Peak signal-to-noise ratio (PSNR) and Structural Similarity Index (SSIM) values in comparison with other priors. **Novelty:** the proposed priors lead to the most effective results for image deblurring using the Bayesian framework. The proposed method improves the performance by 30% in PSNR and 45% in SSIM values in dB with uniform kernel size 12 * 12 and improves performance by 30 % in PSNR and 32% SSIM with a standard deviation of 3.5. The proposed method enhances the frequency response of the real-time image restoration process. **Applications:** Some important applications include the restoration of medical images such as MRI images, CT images where the intensity of these radiations is maintained to avoid damage to human organs. Remote sensing images captured through drones at a specified time cannot be retaken and hence restoring such images is very important. Similarly restoring images from CCTV footage, astronomical images.

Keywords: Blind Image Deblurring; Maximum a Posteriori Estimation; Image priors; Regularization; Structural Similarity Index (SSIM) and Peak signal-to-noise ratio (PSNR)

1 Introduction

In many image restoration and image deblurring algorithms, the image deblurring limitation assumes that there exists a linear shift invariant blur kernel caused due to the degradation process, also known as point spread function (PSF). If PSF is not known, the limitation is termed as blind image deconvolution. In the recent times, blind image deconvolution techniques capable of handling a large motion blur have been designed. The idea of a space invariant blur cannot be generalized. For example, if the camera shakes when a picture is taken, a space-variant blurring occurs due to non-negligible depth variation. The recorded picture is blurred version of real image representing the actual scene in most of the imaging applications. Blurring is caused due to various reasons like optical aberrations, atmospheric distortions, averaging on pixel site on sensor, motion of objects/persons in the scene and motion of camera. Image restoration aims in recovery of real image from a single or a set of recorded images. The problem of restoration is ill-posed and requires techniques of regularization to effectively restore the image.

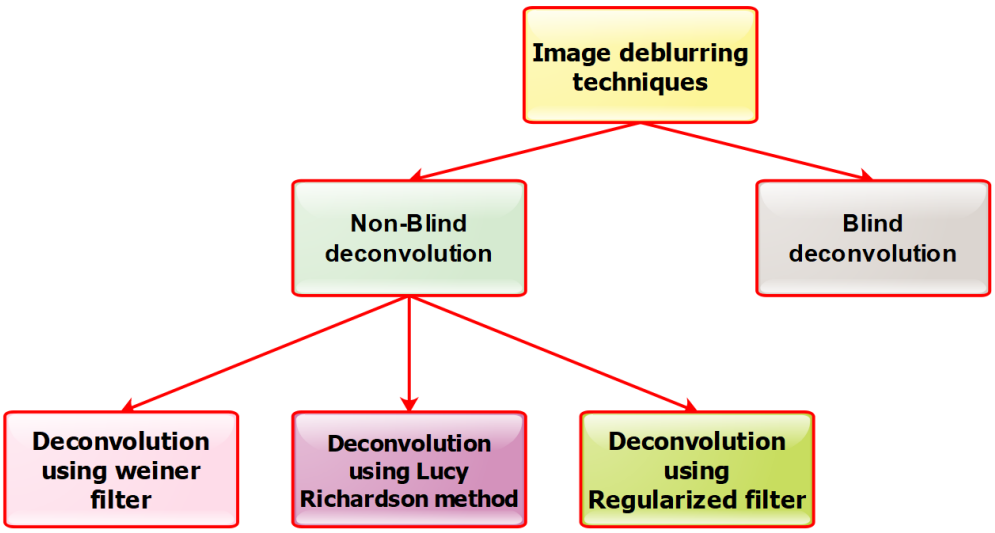

Fig 1. Broad Classification of Image Deblurring Techniques

Figure 1 shows the broad classification of image deblurring techniques, with no knowledge of the point spread function the recovery of the original image constitutes the blind deconvolution. The main objective of the Image Restoration (IR) technique is the recreation or the retrieval of the original sharp image through the perception of the degradation affecting the blurred image. Natural images caught under uncontrolled environmental conditions undergo constant degradation leading to unique image degradation parameters because of flaws in the capturing and imaging cycles. These kinds of degradation can be either variant with respect to space or either invariant with respect to space. The current research work centers more towards invariant blur functions or degradations which are space invariant. The degradation affecting any image might be characterized into two significant classes i.e., Blur and Noise. Images might be blurred because of environmental disturbance, defocusing of the focal point, deviation in an optical framework, relative movement among the imaging framework and the original scene. An automatic image deblurring is a goal of extraordinary practical interest to the upgrade the images in digital photographs, captured through digital cameras or camcorders for numerous applications such as in stargazing, tomography, remote sensing, biomedical imaging, movement following applications, and so on. Image deblurring techniques can be broadly classified into two types: blind and non-blind image deconvolution. In case of non-blind strategies data regarding the blurring channel is known. Blind Deconvolution is the recovery of the original image with unknown blur channel which leads to issues relating to unknown parameters, for example when the captured image is assessed from the perceptions of degradation, the specific data regarding the degradation and also noise isn't accessible. Blind deconvolution issue is exceptionally trying as it is difficult to derive the original sharp image and the degradation parameters from just a captured picture. The strategy which is explained in this work addresses image deblurring techniques of the second kind. In most practical situations, the reactive parameters of a blur, additionally known as Point Spread Function (PSF), isn't known with acceptable accuracy. Non-blind deblurring algorithms are extremely sensitive to mismatches among PSF utilized in the algorithm and a true or valid PSF, helpless information on the blurring PSF typically tends to the lesser effects of deblurring. Through Blind Image Deblurring

(BID) the true or the valid PSF is estimated hence the probability of mismatches caused due to the variations in the degradation parameters utilized by the algorithm and the valid PSF is reduced. The main issue in solving the blind deconvolution problem is its illposedness. The problem is illposed due to the lack of uniqueness and steadiness of the solution caused due to infinite numbers of arrangements (real picture + blurring channel) that are viable for the degraded image. The outline of BID techniques is referred from [1]. The unique quality of the scene or the uniqueness of the captured image can be used to reduce the ill posedness of the problem. Various such techniques have been proposed, for example in [2] a unique filter is applied on the deblurred images to recover the parts which are in focus and another image is used to recover the portions which are not in focus. Vahid Saffari et al. [3] introduces the novel nonparametric regression technique for the deblurring of blurred and noisy images which depends on the idea of the LPA (Local Polynomial Approximation) of an image with the consideration of Intersecting Confidence Intervals (ICI) which is adapted to characterize a versatile changing parameter i.e., sizes of window in an LPA assessor. Mean Curvature (MC) Regularization is used to enhance the quality of deblurred images. This regularization method has been less popular compared to the more general image regularization models due to the complexity in solving the MC mathematical model which comprises of higher order derivatives. Faisal Fairag et al. [4] propose a two-level method to solve this problem where the mathematical model is split into two steps, the first step forms a nonlinear system including the higher order derivatives and the second step is a large problem with low order derivatives. The authors show that this MC regularization model results in effective image deblurring. Xiao Yuan et al. [5] propose the use elastic-net regularization as a rank prior. They use salient edge structures estimated from intermediate images along with the elastic net regularization technique which acts as a prior to guide the algorithm to estimate the true blur kernel. Image Deblurring focused on specific objects can use their unique features as priors to improve the deblurring result. One such example is the use of license plate features as a prior in deblurring images of license plates from surveillance cameras at traffic signals. Chenping et al. propose an image deblurring model which uses the features of the license plate as a prior in an Lp norm based sparse regularization model. Since the deblurring is focused only on the license plate, the features of the license plates act as a vital prior in deblurring the degraded license plate images. to gives a way to consolidate earlier information in investigation. Chenping Zhao et al. [6] propose an image prior based on weighted L1-norm regularization. They claim the L1-norm is better suited to remove noise in smooth regions compared to the L2- norm, which is more suited for noise removal in the edges of an image. Figure 2 shows the image deblurring process using Bayesian methods. Figure 2(a) Shows the data analysis procedure stages for non-blind image blurring. Figure 2(b) shows kernel estimation for blind image deblurring and Figure 2(C) Shows the image deblurring based image to image intensity restoration regression process.

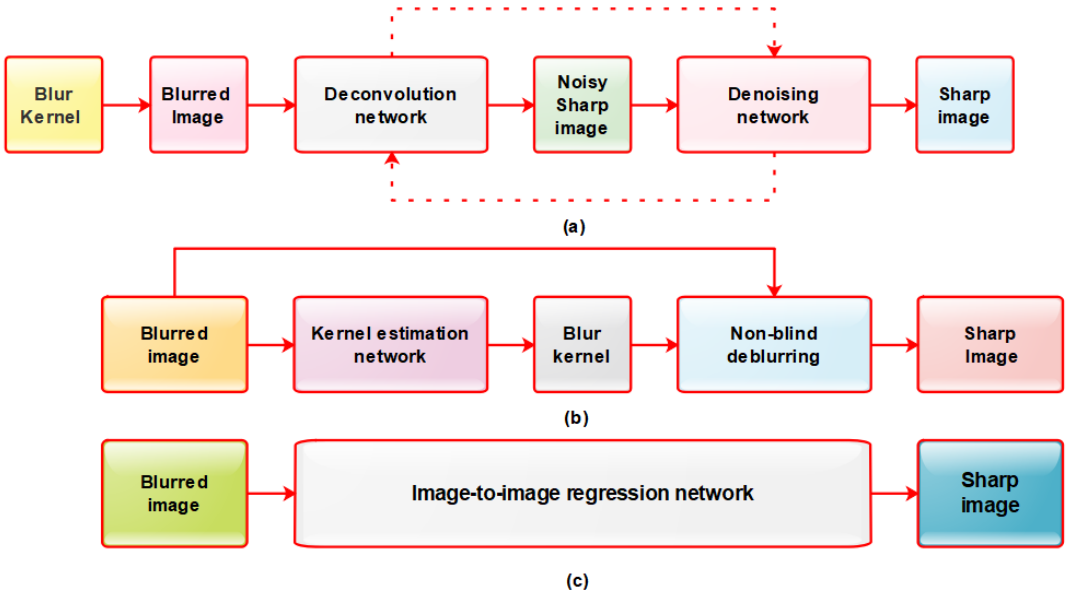

Fig 2. Shows the image deburring process using Bayesian analysis process. It is divided into three steps as shown in figure .2(a), 2(b) and 2(c).

Numerous image processing applications have evolved in various fields in recent times. J. Anger, G. Facciolo et al. developed a graph structure to analyse the constraints caused due to delays and describe the objectives related to cost in an embedded system[(7)]. Zhenhua Xu,. Propose a two-tone image prior which converts the latent image in its intermediate stage into a piecewise constant image comprising of only two grey levels[(8)]. Shao Wen-Ze et al. Propose social tracking method using deep learning to classify the event conduction[(9)]. Fang Dong et al. Make use of the valence arousal dimension space of an image to represent its emotions by predicting the continuous probability distribution of the image[(10)]. P. Blomgren, et al. Propose a microblog filter method designed using the distinguishing factors of the multiple views of the surroundings in the embedding method[(11)]. A new concept was proposed to model images which is pertinent to various image processing application[(12)]. Neural network is used to design a recognition classifier, which uses peripheral and partial Central auditory models. These neural processing models facilitate a speech recognizer comprising of an acoustic pre-processor in the front end to function effectively as a classifier[(13)]. A. Chambolle, P.L. Lions et al. Use simultaneous textual and visual information to assess the relevance and similarities in images which are tagged by the users[(14)]. Po-Wen Hsieh et al. use discriminative classifiers to recognise the core saliency of different objects in an image. Discriminative classifiers are detected or learnt by using a multistage training paradigm[(15)]. In this paper, the true blur kernel and its factors are derived from a blurred image to recover the original image. The novel strategy implemented to derive the blur kernel. It depends on the particular distortion brought about by the distorting administrator in the Fourier range sufficiency of a picture. A format dependent on a few blurred pictures has been created for both kinds of Gaussian and uniform blurred effect. The range of Fourier amplitude in loud obscured picture is compared with the formats to distinguish the blur model. Major factors of the blur are additionally decided based on the Fourier range sufficiency threshold picture. Along with this assessed blur model and factors value, an obscuring channel PSF is built, which is utilized for getting the picture gauge (i.e., deblurred picture) from a blurred picture. Because of the poorly presented nature of IR, earlier information on common pictures can be utilized to minimize the IR issue.

The framework is executed and tests are led with a blur factors such as 7, 9 and 11 for the blur effects of Uniform and factors like 2.5, 2.9, 3.3 has been utilized for the blur effects of Gaussian. The PSNR (Peak Signal to Noise Ratio) and SSIM (Structural Similarity Index Measure) are the two kinds of exhibition estimates utilized here. (PSNR) and (SSIM). Through the outcomes acquired very well, it is noted that the proposed redundant and sparse priors (ASDS) generate results which are more accurate and aesthetically pleasing compared to the more recent methods.

2 Maximum A Posterior (MAP) estimation for the Image Deblurring Problem

In this section the basic image deblurring problem statement is first defined. The general Bayesian mathematical model and its use in the image deblurring model is described. And the gain in using the MAP method for the blind image deblurring problem is shown. The further part of the section relates the statistical characteristics of the most common blur models such as the Gaussian and the Uniform blur model. The most common image priors used in the MAP model is briefly explained.

The general mathematical expression for the image degradation and restoration model is given below

$$b = h_f * a + w \tag{1}$$

Where b and a represents the degraded image and original sharp image respectively, the inevitable noise in the system is represented by w as it is additive in nature it is mathematically represented through a summation. h_f represent the PSF of blurring operation and * represents the convolution operation[(16–19)].

Another alternative method of representing equation 1 will be carried out by depicting it through its spectral equivalent. Under the influence of Discrete Fourier Transforms the frequency domain equivalent of equation 1, is derived as below:

$$B = H_f A + W \tag{2}$$

The capitals in the equation 2 represent the Fourier Transforms of a, b, h_f, and w. In the practical case, the spectral representation is commonly adapted because of its accurate implementations of the restoration filters in a Fourier domain. In case of deblurring under the influence of Discrete Fourier Transforms the blur kernel estimated is responsible for noise generation. Prior information on natural images is utilized to minimize the random noise issue.[(20)] Bayesian methodology gives the way to join prior information in data investigation. Bayesian investigation always evaluates over the circumstance of posterior probability that describes the level of one's certainty with the involvement of circumstances provided. The law of Bayes states that the probability of posterior is directly proportional to the result of probability and probability of prior. The probability incorporates the data which is provided through new information. Prior information communicates the level of certainty involving the circumstance previously and the information is taken to effectively estimate the unknown. Statistical analysis is

conducted in order to increase the information involving the captured image. The current image deblurring problem statement can be described using the Bayes' law as:

$$P_d\left(a \mid n_d\right) = \frac{p_d\left(n_d|a|\right) p_d(a)}{p_d\left(n_d\right)} \tag{3}$$

Posterior is represented as $P_d\left(a \mid n_d\right)$ because of its effects in the examination. It will be the conditional probability of a which gives a new information n_d. The probability $p_d(a)$ is also known as prior because it addresses a condition of information before the trial. The amount of $p_d(n_d|a|)$ is the probability, which communicates the probability of information d given a specific $'a'$. The probability is typically received from a model for anticipating the information, given a, just like a noise in the probabilistic model. The term used in denominator p (d) might be viewed as unity just for standardization process. As standardization accessed from different parameters, Bayes' law is frequently composed as a proportionality, denoting the denominator[21,22].

Even though posterior probability explains the condition of certainty regarding possible image completely, it is required to choose the individual "image result" or reconstruction. A similar selection will be that image which improves the probability of a posterior that is well-known as maximum posteriori (MAP). From the known data b, the posterior of an image is described by Bayes law (3) under the influence of proportionality

$$p_d(a|b)\alpha p_d(b|a)p_d(b|a)p_d(a) \tag{4}$$

In which $p_d(b|a)$ is the probability of a mentioned information and a is likelihood and $p_d(a)$ will be prior or earlier probability of an a. The posterior probability density function of a negative logarithm is stated as:

$$\log\left[p_d(a \mid b)\right] = \varphi(a) = \Lambda(a) + \Pi(a) \tag{5}$$

In which the beginning term arise through a likelihood and next term through the prior probability.

Likelihood has been mentioned under the assumed probability density function in a measurement of fluctuations regarding their predicted value (without noise). The negative log will be just a half of chi-squared for the additive uncorrelated Gaussian noise assumptions

$$-\log\left[p_d(b \mid a)\right] = \Lambda(a) = \frac{1}{2}\chi^2 = \frac{1}{2\sigma_w^2}\left|\left|b - ha\right|\right|^2 \tag{6}$$

Selection of likelihood function must depend on a practical statistical characteristic of the image, a statistical characteristic measurement of noise or a deterministic behavior of the blur kernel which is either known or predicted through statistical analysis. The restored image can be estimated from the equation (7) below:

$$\widehat{A} = \underset{a}{argmin}\frac{1}{2}\left|\left|b - hd\right|\right|_2^2 + \lambda\,\pi(a) \tag{7}$$

Where a= restored image and λ= parameter of regularization.

2.1 Image Priors in MAP

The selection of the right prior is crucial for effective restoration of the original image. Five of the most common priors used in the MAP mathematical model are discussed in this section Tikhonov (L2), Sobolev, Total variational (TV), Sparse, Sparse and redundant prior[23–27].

2.1.1 Tikhonov and Sobolev Priors

The Tikhonov and the Sobolev priors are discussed in the same section due to their interdependence in image deblurring applications, as explained further in this section. The Tikhonov prior is more commonly called as L2 norm prior. It mainly depends on criteria that, the energy available in images are bounded, whereas the noise in the image is unbounded. The restored image can be derived from equation 13.

$$\begin{aligned} &\widehat{a} = \arg\min_x \left|\left|b - h_f * a\right|\right|_2^2 + \lambda\left|\left|\left|x\right|\right|_2^2\right| \\ &Where\ \ \|\,a\,\|_2^2 = \left(\sum_i |a_i|^2\right)^{1/2} \end{aligned} \tag{13}$$

The solution to the above equation is computed in the frequency domain as given in equation 14. Due to the filtering operation which is diagonalized over the Fourier domain.

$$\widehat{A}\ (\omega) = \frac{B(\omega)\widehat{H_f}(\omega)}{\left|\left|\widehat{H_f}(\omega)\right|\right|^2 + \lambda} \tag{14}$$

In which $\widehat{A}\ (\omega), B(\omega), \widehat{H_f}(\omega)$ represents the frequency domain equivalent of the restored image, captured blurred image and the blur function (PSF) respectively[28–32]. As the L2 regularization will not conduct any denoising, in order to eliminate noise more frequencies in a blurred picture can be penalized by using Sobolev prior. The Sobolev is prior stated below:

$$\pi(a) = \sum_i ||\nabla a(i)||^2 = \sum_w S(\omega)\,||A(\omega)||^2.$$

Where $S(\omega) = ||\omega||^2$

As this prior is applied in the Fourier domain, the solution to the deblurring with a Sobolev prior can be normally framed with the Fourier coefficients as given in equation 15:

$$\widehat{A}(\omega) = \frac{B(\omega)\widehat{H_f}(\omega)}{||\widehat{H_f}(\omega)||^2 + \lambda S(\omega)} \tag{15}$$

2.1.2 Total Variation Prior (TV)

Regularization of Sobolev significantly reduces noise in the image but it causes blurring in the image edges. The TV prior[33] is capable of reconstructing the sharp edges of the image. The TV prior is given as:

$$\pi(a) = \sum_i ||\nabla a(i)|| \tag{16}$$

Concerning the energy of Sobolev, it essentially measures L1 norm rather than L2 norm, the L1-norm functional is derived by removing the square as shown in equation (16). The L1-norm is the addition of absolute values of the image intensity components[34,35]. The TV prior (a) of an image a is not a smooth function, hence it needs the utilization of optimization techniques to be applied in a minimization objective function such as the MAP for regularization. Another method is to make use of the smooth absolute value instead of the absolute value of the image intensity. The expression for the smoothened TV prior is given as:

$$(a) = \sum_i \sqrt{||\nabla a(i)||^2 + \varepsilon^2 + 1} \tag{17}$$

As ε draws near to zero, the smoothened values turn out to be nearer to the original TV (total variation), hence optimization is more complicated. As the ε value increases, the smoothed energy turns out to be nearer to Sobolev energy, thus degrading the image edges. Since the TV prior is non-quadratic, it cannot be expressed in the frequency domain. Hence, to optimize an objective function making use of a TV prior requires an iterative method such as the gradient descent.

The expression to apply the gradient descent optimization method for image deblurring is shown in equation (18). Initially the deblurred image 'a' assumed the intensity values of the blurred image and with each iteration the intensity values are updated to derive the restored sharp image.

$$a_{(k+1)} = a_{(k)} - \gamma(h_f * (h_f * a_{(k)} - b) + \lambda\ Grand\ (a_{(k)})) \tag{18}$$

In which $a_{(k+1)}$ represents the value of 'a' in the current iteration and $a_{(k)}$ represents the value of 'a' in previous iterations.

The same procedure is repeated until the final stopping criteria is met. The stopping criteria is fixed to a total number of iterations in this case. The standard test image of a cameraman deblurred using the TV prior is shown in the Figure 8(d).

2.1.3 Sparsity Prior:

Prior of sparsity involves a synthesis dependent regularization, shown in Figure 8(g). An inadequate set of coefficients $(x_m^*)_m$ in an edge $\varphi = (\varphi_m)_m$, i.e., wavelet change which is applied in the blurred picture. Subsequent to applying the wavelet change, the energy will be present in lower number of coefficients (low-low band coefficients are taken). The L1-standard of the inadequate arrangement of coefficients is taken as the prior. The deblurred picture x can acquired from

$$a^* = \underset{a}{argmin}\frac{1}{2}\ \left|\left|b - h_f * a\right|\right|^2 + \lambda||< a, \varphi_m >||_1 \tag{19}$$

$\|\langle a,\varphi_m\rangle\|_1 = \sum_m |\langle a,\varphi_m\rangle|$, b is the blurred picture and h_f is the blurring filter (PSF). In order to solve this non smooth optimization issue, iterative soft thresholding is utilized. Series of images a^s are computed by the equation 19.

$$a^{(s+1)} = S^{\varphi}_{\tau\lambda}(a^s - \tau h_f * (h_f * a^{(s)} - b)) \tag{20}$$

Where $\tau < \frac{2}{||h_f * h_f||}$

2.1.4 Sparse and Redundant Prior

The proposed image deblurring algorithm distinguishes the blur parameters from the blurred image. This helps in recovering the blur model from the captured blurry image. The knowledge of the blur parameters is very useful in solving the inverse problem of extracting the unknown blur model from the captured in blurred image. These prior thinks about the substance that can fluctuate fundamentally over various pictures or various patches in a solitary picture. The ASDS (adaptive sparse and redundant priors) strategy[35] utilizes these prior. These technique takes in different arrangements of bases from the pre collected dataset of model picture patches and afterward for an offered fix to be handled, one bunch of bases are adaptively chosen to describe the nearby local sparse domain. With the equation (21).

$$a = \phi\alpha \tag{21}$$

Where $\Phi = [\phi_1, \phi_2, \phi_3, \phi_4, \ldots\ldots\ldots\phi_m]$

$$\widehat{\alpha} = \underset{\alpha}{argmin}\{||b - H_f\phi\alpha||_2^2 + \lambda||\alpha||_0$$

Where the L0-norm counts the quantity of non-zero coefficients in a vector α. Once $\alpha\hat{}$ is acquired, $'a'$ would then be able to be assessed as $\widehat{a} = \phi\ \widehat{\alpha}$. The L0-minimization is a NP-hard combinatorial inquiry issue, and is typically tackled by ravenous calculations. Set of minimized sub-word references from top notch model picture patches are gotten the hang of utilizing principal component analysis (PCA) strategy. For a picture fix to coded, the best sub-word reference which is generally applicable for a given fix is chosen.

In case that, $(\phi_k\}, k = 1,2,3,4\ldots\ldots\ldots\ldots K$, will be the set of K orthonormal sub-dictionaries. Let $'a'$ be an image vector, and $a_i = V_i a,\ i = 1,2,3,4,5,\ldots\ldots\ldots\ldots N$, be the ith patch (size: 8×8) vector of $'a'$, where V_i is a matrix extracting patch a_i from $'a'$. For patch a_i, suppose that a sub- dictionary ϕ_{ki} is selected for it. Then, a_i can be approximated as $\widehat{a} = \phi_{k_i}\ \widehat{\alpha_i}$, $||\ \alpha_i||_0 \leq\ U$ via sparse coding. The entire picture $'a'$ can be reframed by averaging all the reframed patches $\widehat{a_i}$, is arithmetically given as:

$$\widehat{a} = \left((\sum_{i=1}^{N} V_i^U V_i)^{-1}\right)\sum_{i=1}^{N}(V_i^U \phi_{k_i}\alpha_i) \tag{22}$$

3 Proposed Method

The effective estimation of the true blur kernel is vastly dependent on the selection of the right prior. Numerous priors have been designed by various research scholars to explicitly and implicitly meet the required criteria of selection of right parameters in the recovered sharp image. The captured blurry image though assumed to be degraded by a space invariant blur function, the effects of the blur are not constant on the entire image. For example, the effect of blur is more prominent on an object in motion in the image scene whereas it is less prominent on the background objects of the image captured. The use a generic and constant prior over the entire image does not result in effectively recovering such variations in degradation. Hence, we propose adaptive image priors which vary according to the deblurring requirements of the image. A Novel Image Prior based on hybrid regularization techniques to adaptively induce sparsity is proposed in this paper.

3.1 Spectral Characteristics of Blurring

The proposed Adaptive priors are set to vary based on the spectral characteristics of the image. The spectral characteristics of the image provide insight into the nature of the blurring caused, the effect of possible additive noise. Considering blurring as an operation we can assess that it suppresses various spectral components of an image. The range of spectral components suppressed due to blurring depends on the type of blur acting on the image. For example, the below image in Figure 3(a) shows the spectral components of an original sharp image, Figure 3(b) shows the spectral components of the same image when it is blurred using a synthetic uniform blur, similarly Figure 3(c) shows the spectral components of the same image blurred using a synthetic Gaussian blur. The spectral components of various blurs are empirically analyzed to understand their effect on a captured blurred image. The statistical data from these experiments are used in our algorithm to vary the adaptive priors.

3.1.1 Blur Template Identification

A layout of blur is developed through the frequency domain representation of a few blurred images. Initially the Fourier range adequacy of blurred images and their threshold is estimated. Subsequent to thresholding, the morphological activity[36] is conducted on the resultant image. A morphological activity applies an organizing component to a data image, giving an output image of a common size. Under the activity of morphology, an estimation of each pixel in an output image based on the correlation of comparing pixel in an info image along with its neighbors. By taking a state and size of the area, morphological activity which is sensitive to explicit shapes in an information image is developed. Hence, enlargement is done with a disk structuring component. A structuring element is a network composed with just 0's and 1's can have any self-assertive structure and size. The pixels of estimations 1 characterizes an area. Widening adds pixels for the limits of figures in a picture. The quantity of pixels included or eliminated through the items in a picture relies upon a size and state of structuring component utilized to deal with the picture. The estimation of an output pixel is a greatest estimation of a relative multitude of pixels in an input pixel's area. From the double picture, if any of a pixel is assigned to a value 1, an output pixel is assigned to 1. Widening is carried in order to define the limit pixels to interface the overall white areas.

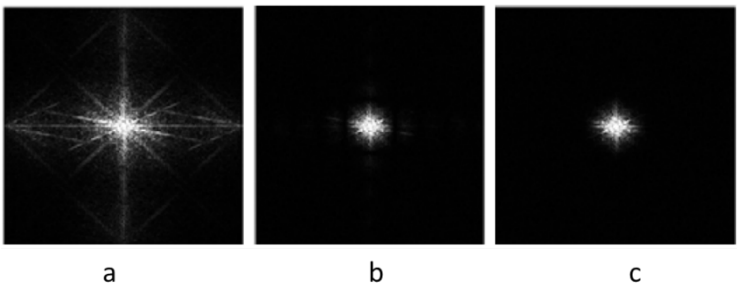

Fig 3. Blurring suppresses certain frequencies in an image (a) the frequency spectrum of an original image which is uncorrupted by blur (b) the frequency spectrum of the same image which is blurred by a uniform blur (c) the frequency spectrum of the same image which is blurred by a Gaussian blur.

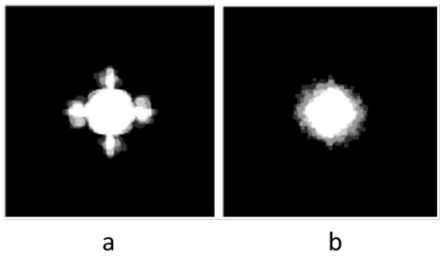

Fig 4. The appearance of a point spread function or a blur kernel is depicted for (a) Uniform blur (b) Gaussian blur

Through every blurred image, an enlarged image is developed. A mean image of this enlarged Gaussian blurred image is made and it is considered as the format for distinguishing Gaussian blur. Likewise, a format for unique blur ID is developed. The point spread function which follows a Gaussian distribution is given as:

$$h_f(n_1, n_2) = \frac{1}{2\pi\rho^2} exp(-\frac{n_1^2 + n_2^2}{\rho^2}) \tag{8}$$

Where ρ^2a variance gaussian functional parameter of the PSF, Figure 5 shows the gaussian functional Fourier transform and its absolute value.

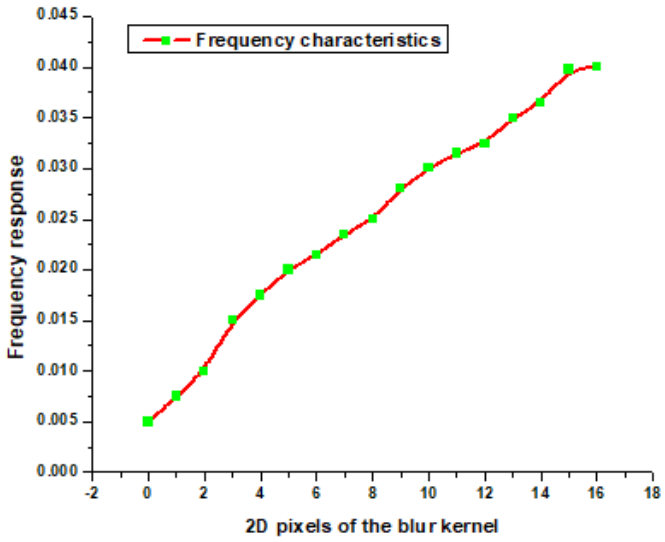

Fig 5. Frequency response with respect to gaussian Point Spread Function (PSF).

The uniform rectangular blur is mathematically represented by the below equation

$$h_f(n_1, n_2) = \left\{ \begin{array}{l} \frac{1}{s^2}, |n_1| < \frac{s}{2}, |n_2| < \frac{s}{2} \\ 0, \\ \text{elsewhere} \end{array} \right\} \tag{9}$$

In which $'s'$ gives the area of smoothing. The characteristics of frequencies in equation 8 are represented in Figure 6.

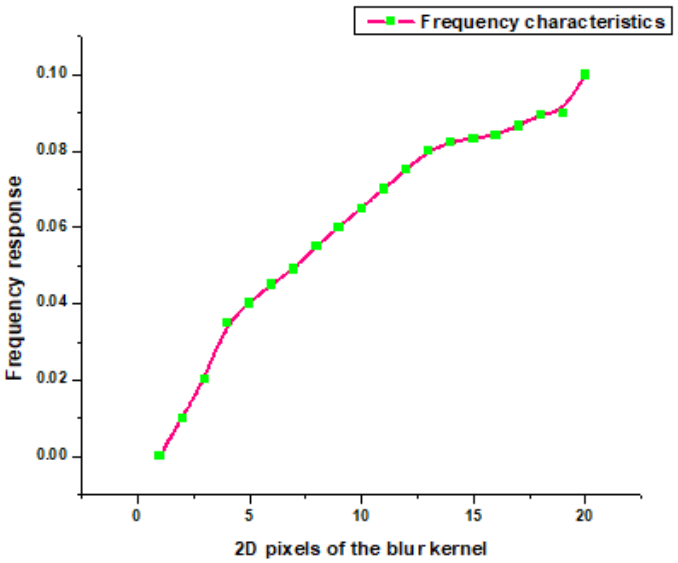

Fig 6. Frequency Response with respect to uniform blur kernel

Prior information regarding some deblurring function and its factors will be of essential significance in a deblurring the distorted image[36–42]. This work implements a novel strategy for image enhancement by identifying the type of blur through the spectral components of the captured image. As the Fourier range of an image is affected under the influence of blur, this technique distinguishes the blur based on its Fourier amplitude range. By recognizing the kind of blur, its factors are likewise removed from a Fourier range threshold image through the use of appropriate adaptive priors. Similarly, formats for distinguishing the popular synthetic blur models such as Uniform blur, disk blur and motion blur are developed.

3.2 Estimation of the True Blur Kernel through the Proposed Method

In case of deblurring, initially the Fourier range sufficiency of a deblurred image is considered. The spectral components of the image greater than the estimated threshold is decreased through normalization. This image is further dilated, this dilated image is compared with the different blur templates derived in the previous section. The comparison is done through subtracting the dilated image with each of the blur templates identified. These difference images are further processed to check which one of them has the least number of non-zero elements. The blur template with which the dilated image has produced a difference image with the least number of non-zero elements is identified as the blur affecting the captured image. In an event that the blur affecting the image is some other type of blur then the number of non-zero elements in the difference image will be very high. Even in situations when none of the existing blur templates represent the type of blur which has affected the distorted image, one of these templates will have a minimum value compared to the others and hence it will be chosen as the blur affecting the captured image. Hence, to keep away from this incorrect selection a constraint is adapted such that the minimum value required for blur template selection is a constant.

Since Gaussian and uniform blur are statistical blurs, their variance is measured using the dimensions of the PSF, for the Gaussian blur the variance is proportional to the radius of a middle white part of the PSF. Fluctuations have impact over the span of a middle white part of the dilated image. i.e., radius of the middle white region of the PSF is proportional to the level of variance the Gaussian distribution follows. The value of variance relating to radius of the PSF is figured as mentioned below:

$$Value = (\frac{r - L_r}{U_r - L_r}) \tag{10}$$

$$Variance = (0.5 * Value) + L_r \tag{11}$$

Where, U_r is the upper radius and L_r the lower radius of the PSF show's the analysis of variance range and radius. Consider radius >55, the variance range manipulated by using euaqtion.12.

$$\begin{aligned} Value &= 1 - ((\frac{r - 55}{62 - 55})) \\ Variance &= (0.5 * Value) + 1 \end{aligned} \tag{12}$$

In case of uniform blur, height and breadth of a middle white portion is determined and least of it has been considered as a length[43]. On the off chance that length is in the reach or not exactly a particular worth, at that point the portion size comparing to that is chosen. Along with these assessed blur type and blur factors, the blurring channel PSF is developed as indicated in segment. These assessed PSF parameters are utilized in the image deblurring algorithm to vary accordingly the regularization norm of the hybrid image deblurring algorithm.

3.2.1 Proposed Image Deblurring Algorithm

The proposed image deblurring algorithm is implemented in MATLAB. The MAP mathematical model is used for implementation due to its reduced computational complexity. The main reason for using the MAP model is due to its readiness in incorporating the image priors or the prior information regarding the image in its estimation of the true PSF. The algorithm is designed utilizing the MAP mathematical expression shown in equation (6). The algorithm is designed to adaptively vary the image priors based on the spectral analysis of the captured image, that is described in the previous sub section. Here the regularization term used is the L_p Norm Regularization. By varying the p value, the sparsity induced in the various image region varies. Hence this varies the image prior accordingly. The novel image prior so chosen from our algorithm is called the Sparsity through Adaptive Priors (SAP).

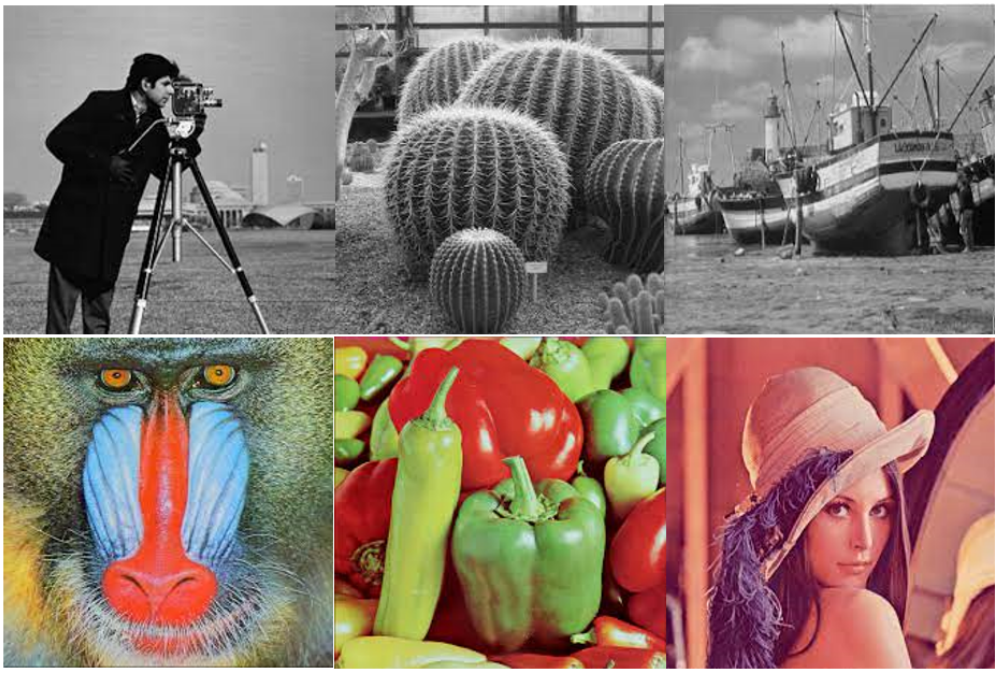

Fig 7. The six standard test images of size 512X512used from top left (clockwise): Cameraman, Cactus, Boat, Lena, Peppers, Baboon.

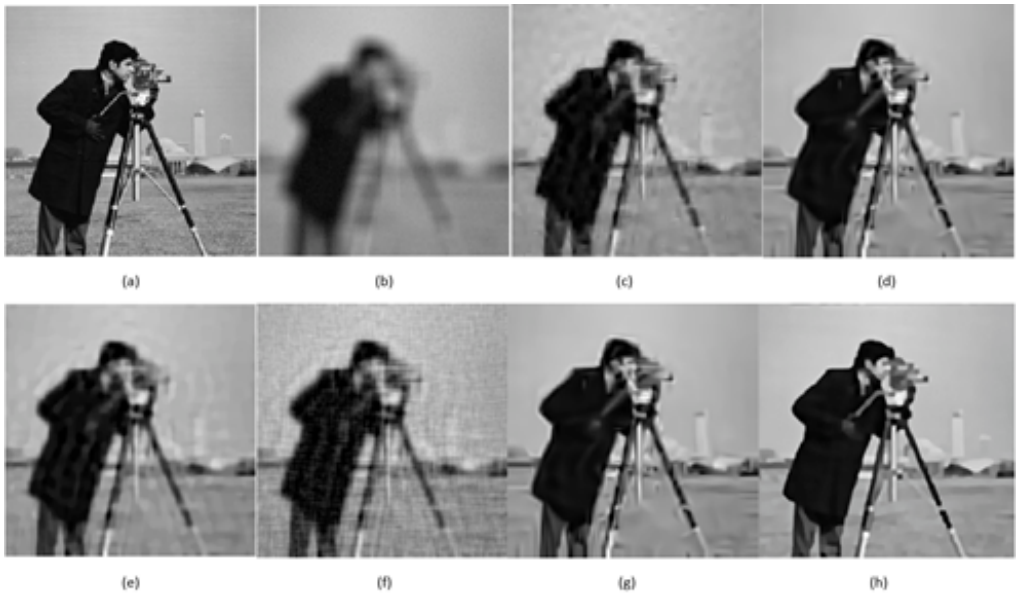

Fig 8. Comparison of image deblurring results of different methods using the standard test image of cameraman: (a) Original Image (b) Image blurred through Uniform Blur (c) Deblurred using Tikhonov & Sobolev Priors (d) Deblurred using TV Priors (e) Deblurred usingSparse Priors (f) Deblurred using L1 Priors (g) Deblurred using Sparse and Redundant Priors (h) Deblurred using the proposed method (SAP).

4 Results and Discussion

The performance of the proposed novel image prior (SAP) in an image deblurring algorithm using the MAP mathematical model is compared with the popular generic image priors used in the MAP model such as the Tikhonov (L2), Sobolev, Total variational (TV), Sparse, Sparse and redundant prior. Six standard test images are used to compare the performance, which consists of both grayscale and color images. The three standard grayscale test images used are Cameraman, Cactus and Boat. Similarly, the three standard color test images used are Baboon, Peppers and Lena shown in Figure 7. The investigation on performance of the proposed method is done through the use of performance metrics such as the Peak Signal to Noise Ratio (PSNR) and the Structural Similarity Index (SSIM). The test images are synthetically blurred using a Uniform blur of kernel size 12X12. The synthetically blurred images are deblurred using the popular generic image priors and the proposed SAP image prior. The PSNR & SSIM values for the resulting deblurred images using various methods are estimated and tabulated in the Tables 1 and 2. The resulting PSNR & SSIM values are plotted in the graphs shown in Figures 9 and 10.Figure 12

Table 1. The PSNR result analysis in dB of the blurred and restored images blurred with Uniform kernel of size 12x12 and graphical analysis is shown in Figure 11.

Name	SAP	Sparsity	Sobolev	L2	TV	Blurred
Animal	27.10	25.86	24.98	24.68	24.75	21.80
Cactus	26.07	25.02	23.90	23.55	23.72	20.36
Lena	29.98	25.80	24.58	24.25	24.69	21.45
Cameraman	29.32	25.50	23.56	22.85	23.54	19.65
Boat	29.99	26.05	24.55	23.95	24.65	20.48
Building	25.35	23.68	21.56	21.56	21.45	18.69

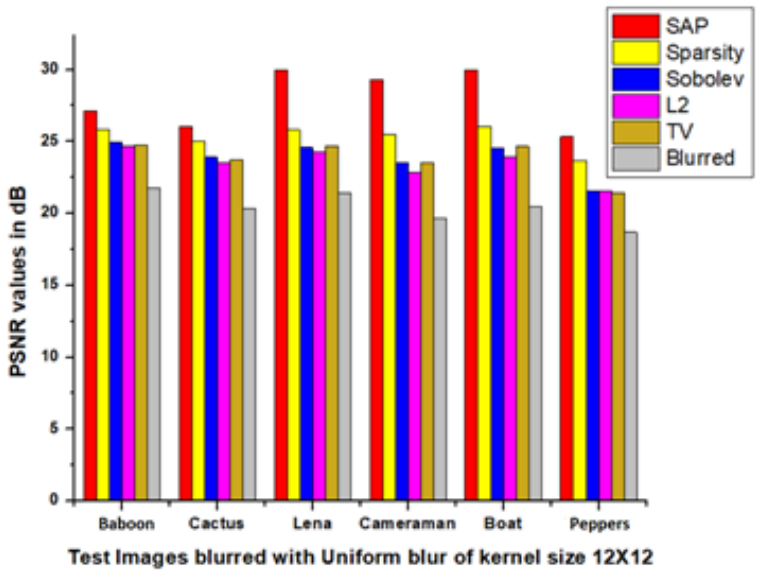

Fig 9. Graphical analysis of PSNR result analysis in dB of the blurred and restored images blurred with Uniform kernel of size 12x12.

Now the test images are synthetically blurred using a Gaussian blur of standard deviation 3.5 and the deblurred results for the same is shown in the Tables 3 and 4. The performance metric values in the Tables 3 and 4 are plotted in the graphs in the Figures 11 and 12 respectively.

The performance of the proposed SAP method is analyzed using real images also, we use naturally blurred satellite image due to atmospheric turbulence and a google image blurred using a uniform blur for the same. The deblurred results for the satellite images utilizing different priors and the google image using different priors are appeared in the Figures 13 and 14, respectively.

Table 2. The SSIM result analysis of the restored images blurred with Uniform kernel of size 12 *12 and graphical analysis is shown in Figure 10.

Name	SAP	Sparsity	Sobolev	L2	TV
Animal	0.789	0.623	0.642	0.610	0.615
Cactus	0.786	0.595	0.580	0.585	0.585
Lena	0.832	0.599	0.595	0.596	0.595
Cameraman	0.956	0.625	0.608	0.605	0.610
Boat	0.865	0.526	0.599	0.580	0.580
Building	0.823	0.590	0.587	0.580	0.578

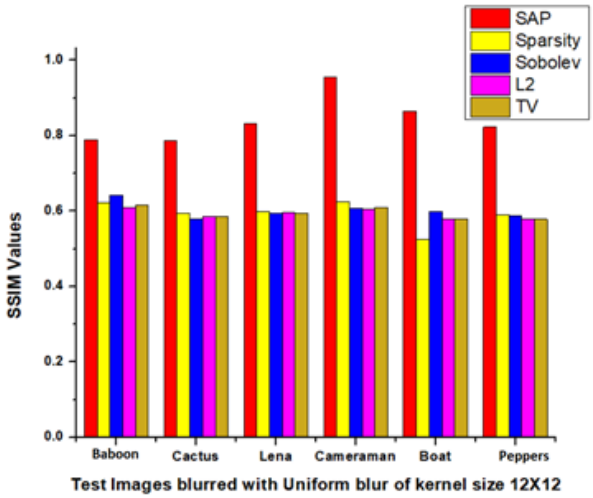

Fig 10. Graphical analysis of SSIM result analysis of the restored images blurred with Uniform kernel of size 12 *12

Table 3. The PSNR result analysis in dB of the blurred and restored images blurred with Gaussian blur of standard deviation 3.5 and graphical analysis is shown in Figure 11.

Name	SAP	Sparsity	Sobolev	L2	TV	Blurring	Estimated Variance
Animal	26.50	25.880.	24.20	24.40	24.70	22.65	2.41
Cactus	25.68	25.30	23.99	23.41	23.75	21.45	2.402
Lena	28.50	25.89	24.70	24.75	24.89	22.34	2.35
Cameraman	25.65	25.29	22.98	22.98	22.90	20.40	2.39
Boat	26.89	25.79	24.45	21.35	24.25	21.50	2.40
Building	23.48	23.10	21.45	21.40	21.20	19.40	2.51

Table 4. The SSIM result analysis of the restored images blurred with Gaussian blur of standard deviation 3.5 and graphical analysis is shown in Figure 12.

Name	SAP	Sparsity	Sobolev	L2	TV
Animal	0.730	0.615	0.613	0.610	0.615
Cactus	0.720	0.578	0.580	0.573	0.578
Lena	0.799	0.597	0.560	0.589	0.598
Cameraman	0.862	0.609	0.608	0.609	0.609
Boat	0.780	0.580	0.581	0.580	0.589
Building	0.762	0.582	0.582	0.579	0.580

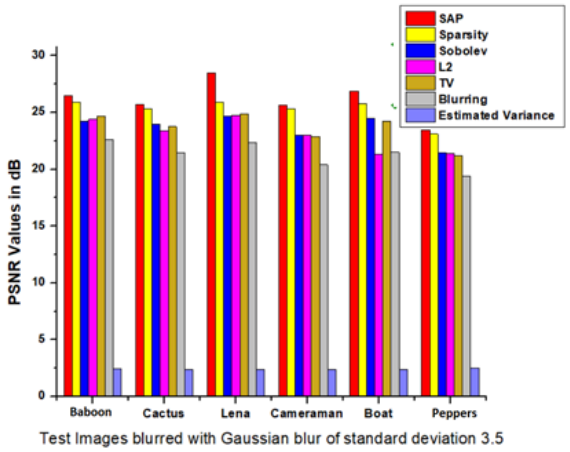

Fig 11. Graphical Analysis PSNR result analysis in dB of the blurred and restored images blurred with Gaussian blur of standard deviation 3.5.

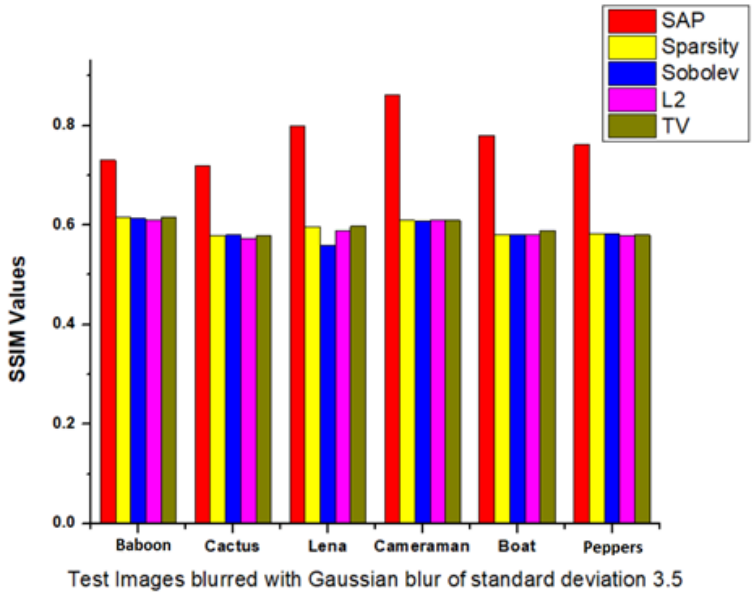

Fig 12. Graphical Analysis SSIM result analysis in dB of the restored images blurred with Gaussian blur of standard deviation 3.5

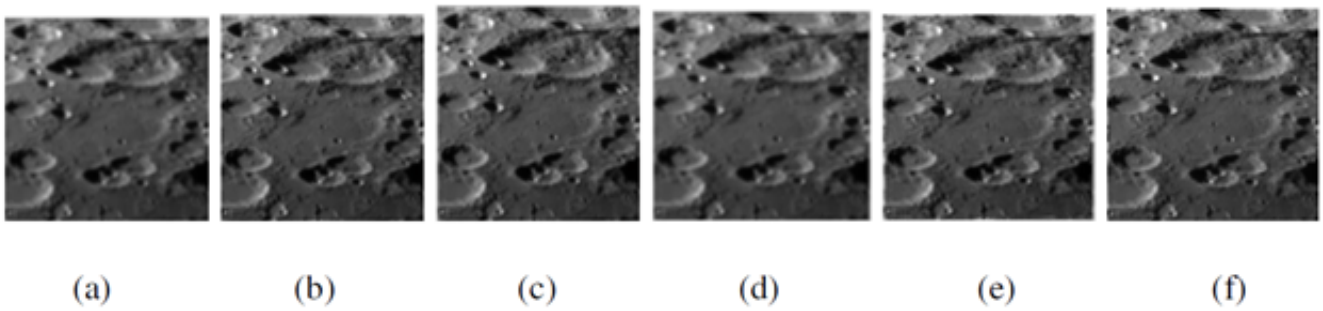

Fig 13. Comparison of image deblurring results of different methods: (a) Captured blurred satellite image (b) Deblurred using Sobolev Priors (c) Deblurred using TV Priors (d) Deblurred using Tikhonov Priors (e) Deblurred using Sparse Priors (f) Deblurred using the proposed method (SAP).

Fig 14. Comparison of image deblurring results of different methods: (a) Original Image (b) Image blurred through Uniform Blur (c) Deblurred using Sobolev Priors (d) Deblurred using TV Priors (e) Deblurred using Gaussian Priors (f) Deblurred using L1 Priors (g) Deblurred using Tikhonov Priors (h) Deblurred using Sparse Priors (i) Deblurred using the proposed method (SAP)

The Figure 15. Shows the performance analysis between existing and proposed methods with respective aspect ratio = 3.32

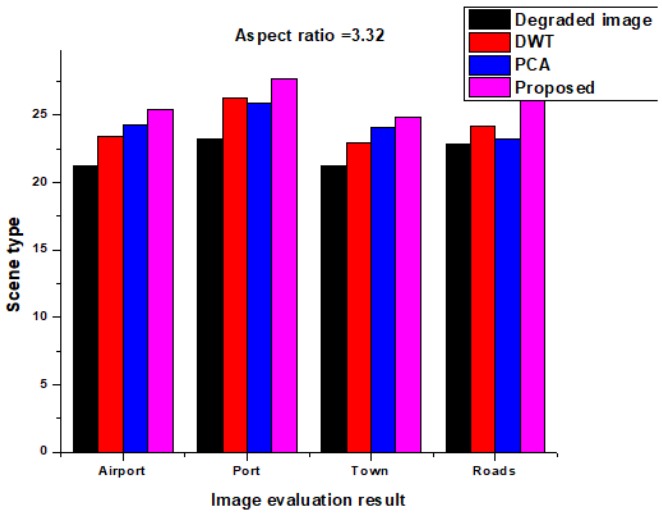

Fig 15. performance analysis between existing and proposed methods with respective aspect ratio=3.32.

As shown in Figure 16 performance analysis between existing and proposed methods with respective to real life blurring image.

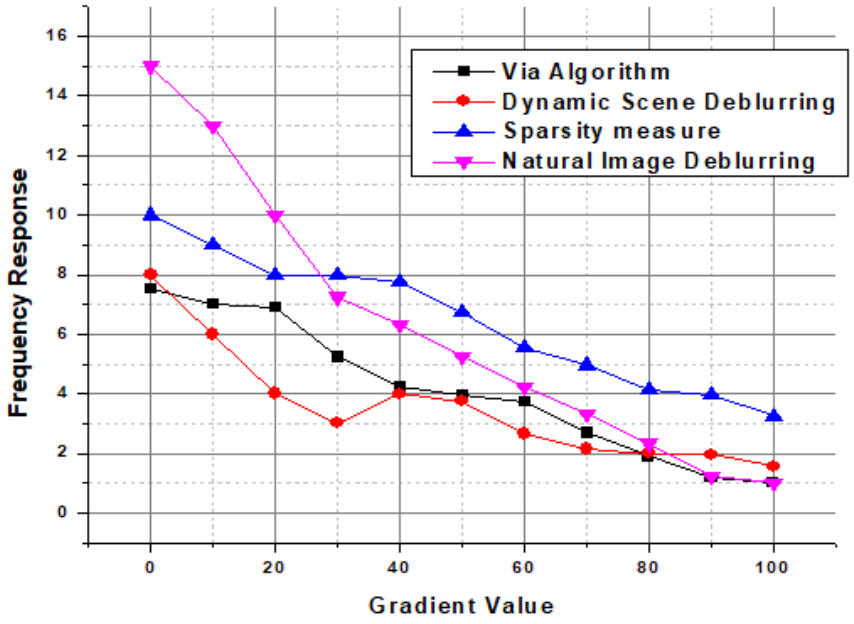

Fig 16. performance analysis between existing and proposed methods with respective to real life blurring image

Table 5. shows the performance analysis of SSIM and PSNR values of various conventional methods with the proposed method.

SI.NO	Reference Number	Methods	Protocol	SSIM (%)	PSNR (%)
1.	(1)	Sparsity	Uniform kernel of size 12x12 (Animal Image)	0.0623	0.2586
	(2)	Sobolev		0.0642	0.2498
	(3)	L2		0.0610	0.2468
	(44)	TV		0.0615	0.2475
	(19)	Blurring		-	0.2180
	(32)	Estimated Variance		-	-
	-	Proposed		0.789	0.2710
2.	(23)	Sparsity	standard deviation 3.5 (Animal Image)	0.0615	0.25880
	(45)	Sobolev		0.0613	0.2420
	(46)	L2		0.0610	0.2440
	(42)	TV		0.0615	0.2470
	(41)	Blurring		-	0.2265
	(40)	Estimated Variance		-	0.0241
	-	Proposed		0.0073	0.2650

5 Conclusion

The proposed method is implemented using the Bayesian MAP mathematical model approach, the novel SAP image priors are incorporated in the MAP model which effectively estimates the blur types and its parameters. Comparison of proposed method with conventional methods with respect to fixed uniform kernel value 12 * 12 , shows that ASP has 27.10 PSNR and 0.789 SSIM value in dB whereas conventional methods PSNR and SSIM values has less value than the proposed method. The proposed blurring filter makes use of sparse and redundant priors to improve constructive PSF efficiency up to 13.06 % as compared to conventional methods. Our method is compared with five other important priors like total variation, sparse, L2, Sobolev in a Bayesian framework. This performance analysis is made utilizing peak-signal-to-noise ratio (PSNR) and structural similarity index [SSIM] by considering sets of blur parameters 7,10 and 12 for uniform blur and parameter 2.6, 3.0 and 3.4 for Gaussian blur. As per the comparison and performance analysis, the sparse and redundant prior gives better results. ASP performance

is improvement is in range of 25 to 30% in PSNR and 40 to 45 % improvement in SSIM values in dB with uniform kernel of size 12 * 12 and ASP performance improvement in range of 28 to 30% in PSNR and 26 to 32% in SSIM values of blurred and regained pictures with Gaussian blur have standard deviation 3.5.

6 Limitation and Future scope

The proposed image deblurring algorithm is implemented in MatLab and hence the execution time of the algorithm is slightly larger when compared to recent image deblurring methods implemented using platforms such C++. The proposed image deblurring model can be extended to a variety of applications such as MRI images and satellite images. Due to its similarity with the problem statement of Super Resolution, the same algorithm can be extended to generate super resolution images.

Acknowledgements

The authors would like to thank JSS Academy of Technical Education, Bengaluru, Visvesvaraya Technological University (VTU), Belagavi and Vision Group on Science and Technology (VGST) Karnataka Fund for Infrastructure strengthening in Science & Technology Level – 2 for all the support and encouragement provided by them to take up this research work and publish this paper

References

1) Mohan K, Chandrasekhar P, Jilani SAK. Object Face Liveness Detection with Combined HOGlocal Phase Quantization using Fuzzy based SVM Classifier. *Indian Journal of Science and Technology*. 2017;10(3):1–10. Available from: https://dx.doi.org/10.17485/ijst/2017/v10i3/109035.
2) Kumaravel S, Sundar KJA, Vaithiyanathan V. Super Resolution Image Reconstruction for Bone Images. *Indian Journal of Science and Technology*. 2019;12(26):1–6.
3) Saffari V, Ghazimoradi A, Alirezanejad M. Effect of Laplacian of Gaussian Filter on Watermark Retrieval in Spatial domain Watermarking. *Indian Journal of Science and Technology*. 2015;8(33):1–4. Available from: https://dx.doi.org/10.17485/ijst/2015/v8i1/71226.
4) Fairag F, Chen K, Brito-Loeza C, Ahmad S. A two-level method for image denoising and image deblurring models using mean curvature regularization. *International Journal of Computer Mathematics*. 2021;p. 1–21. Available from: https://dx.doi.org/10.1080/00207160.2021.1929939.
5) Yu X, Xie W. Single Image Blind Deblurring Based on Salient Edge-Structures and Elastic-Net Regularization. *Journal of Mathematical Imaging and Vision*. 2020;62(8):1049–1061. Available from: https://dx.doi.org/10.1007/s10851-020-00949-6.
6) Zhao C, Wang Y, Jiao H. Lp-Norm-Baesd Sparse Regularization Model for Liscence Plate Deblurring. *IEEE Access*. 2020;8:22072–22081.
7) er´ emy Anger J, Facciolo G, Delbracio M. Blind image deblurring using the lo gradient prior, Image Process. *On Line*. 2019;9:124–142. Available from: 10.5201/ipol.2019.243.
8) Xu Z, Chen H, Li Z. Blind image deblurring using group sparse representation. *Digital Signal Processing*. 2020;102(1-8):1–8. Available from: 10.1016/j.dsp.2020.102736.
9) Wen-Ze S, Yuan-Yuan L, Lu-Yue Y. DeblurGAN+: Revisiting blind motion deblurring using conditional adversarial networks. *Signal Processing*. 2020;168:1–10. Available from: 10.1016/j.sigpro.2019.107338.
10) Dong F, Ma Q. Single image blind deblurring based on the fractional-order differential. *Computers & Mathematics with Applications*. 1960;78(6):1960–1977. Available from: 10.1016/j.camwa.2019.03.033.
11) Blomgren P, Chan TF, Mulet P, Wong CK. Total variation image restoration: numerical methods and extensions. *Proceedings of IEEE International Conference on Image Processing*. 1997;(3):384–387. Available from: 10.1109/ICIP.1997.632128.
12) Cai JF, Ji H, Liu C, Shen Z. Framelet-Based Blind Motion Deblurring From a Single Image. *IEEE Transactions on Image Processing*. 2012;21(2):562–572. Available from: https://dx.doi.org/10.1109/tip.2011.2164413.
13) Candes EJ, Wakin MB, Boyd SP. Enhancing sparsity by reweighted l1 minimization. *J Fourier Anal Appl*. 2008;14:877–905. Available from: 10.1007/s00041-008-9045-x.
14) Chambolle A, Lions PL. Image recovery via total variation minimization and related problems. *Numerische Mathematik*. 1997;76(2):167–188. Available from: https://dx.doi.org/10.1007/s002110050258.
15) Hsieh PW, Shao PC. Blind image deblurring based on the sparsity of patch minimum information. *Pattern Recognition*. 2021;109. Available from: https://dx.doi.org/10.1016/j.patcog.2020.107597.
16) Mohan SC. Adaptive Super-Resolution Image Reconstruction with Lorentzian Error Norm". *Indian Journal of Science and Technology*. 2017;10(16):1–6. Available from: 10.17485/ijst/2017/v10i16/106780.
17) Rajkumar S, Malathi G. A Comparative Analysis on Image Quality Assessment for Real Time Satellite Images. *Indian Journal of Science and Technology*. 2016;9(34):1–11. Available from: https://dx.doi.org/10.17485/ijst/2016/v9i34/96766.
18) Mamta R, Dutta M, and. GA based Blind Deconvolution Technique of Image Restoration using Cepstrum Domain of Motion Blur. *Indian Journal of Science and Technology*. 2017;10(16):1–8. Available from: https://dx.doi.org/10.17485/ijst/2017/v10i16/114303.
19) Janani P, Premaladha J, Ravichandran KS. Image Enhancement Techniques: A Study. *Indian Journal of Science and Technology*. 2015;8(22):1–12. Available from: https://dx.doi.org/10.17485/ijst/2015/v8i22/79318.
20) Suresh G, Rao CS. RST Invariant Image Forgery Detection. *Indian Journal of Science and Technology*. 2016;9(22):1–8. Available from: https://dx.doi.org/10.17485/ijst/2016/v9i22/89227.
21) Uma K, Pallavi AR, Srilatha S. Comparision of Blur Detection and Segmentation Techniques. *Indian Journal of Science and Technology*. 2016;9(S1):1–7. Available from: https://dx.doi.org/10.17485/ijst/2016/v9is1/107619.
22) Singh R, Singh S. Navjot Kaur "A Review: Techniques of Vehicle Detection in Fog. *Indian Journal of Science and Technology*. 2016;9(47):1–4. Available from: 10.17485/ijst/2016/v9i45/106793.

23) Umashankar ML, Ramakrishna MV, Mallikarjunaswamy S. Design of High Speed Reconfigurable Deployment Intelligent Genetic Algorithm in Maximum Coverage Wireless Sensor Network. *2019 International Conference on Data Science and Communication (IconDSC)*. 2019;p. 1–6. Available from: https://doi.org/10.1109/IconDSC.2019.8816930.
24) Alam MZ, Qian Q, Gunturk BK. Space-variant blur kernel estimation and image deblurring through kernel clustering. *Signal Processing: Image Communication*. 2019;76:41–55. Available from: https://dx.doi.org/10.1016/j.image.2019.04.014.
25) Zhang H, Wu Y, Zhang L, Zhang Z, Li Y. Image deblurring using tri-segment intensity prior. *Neurocomputing*. 2020;398:265–279. Available from: https://dx.doi.org/10.1016/j.neucom.2020.02.082.
26) Mahendra HN, Mallikarjunaswamy S, Rekha V, Puspalatha V, Sharmila N. Performance Analysis of Different Classifier for Remote Sensing Application". *International Journal of Engineering and Advanced Technology*. 2019;9(1):7153–7158. Available from: http://dx.doi.org/10.35940/ijeat.A1879.109119.
27) N MH, Mallikarjunaswamy S, Siddesh GK, Komala M, Sharmila N. Evolution of real-time onboard processing and classification of remotely sensed data. *Indian Journal of Science and Technology*. 2020;13(20):2010–2020. Available from: https://dx.doi.org/10.17485/ijst/v13i20.459. doi:10.17485/ijst/v13i20.459.
28) Thazeen S, Mallikarjunaswamy S, Siddesh GK, Sharmila N. Conventional and Subspace Algorithms for Mobile Source Detection and Radiation Formation. *Traitement du Signal*. 2021;38(1):135–145. Available from: https://dx.doi.org/10.18280/ts.380114.
29) Chaitra S, Rekha V, Harisha AM, Madhu TA, Mallikarjunaswamy S. A comprehensive review of parallel concatenation of LDPC code techniques. *Indian Journal of Science and Technology*. 2021;14(5):432–444. Available from: https://doi.org/10.17485/IJST/v13i20.459.
30) Umashankar ML, Anitha TN, Mallikarjunaswamy S. An efficient hybrid model for cluster head selection to optimize wireless sensor network using simulated annealing algorithm. *Indian Journal of Science and Technology*. 2021;14(3):270–288. Available from: https://doi.org/10.17485/IJST/v14i3.2318.
31) Raj KS, Siddesh GK, Mallikarjunaswamy S, Raj KV. Interference resilient stochastic prediction based dynamic resource allocation model for cognitive MANETs". *Indian Journal of Science and Technology*. 2020;13(41):4332–4350. Available from: https://doi.org/10.17485/IJST/v13i41.687.
32) Cui G, Ye X, Zhao J, Zhu L, Chen Y. Multi-frame motion deblurring using coded exposure imaging with complementary fluttering sequences. *Optics & Laser Technology*. 2020;126(106119). Available from: https://dx.doi.org/10.1016/j.optlastec.2020.106119.
33) Cheng S, Liu R, He Y, Fan X, Luo Z. Blind image deblurring via hybrid deep priors modeling. *Neurocomputing*. 2020;387:334–345. Available from: https://dx.doi.org/10.1016/j.neucom.2020.01.004.
34) fang F, Qianting MD. Single image blind deblurring based on the fractional-order differential. *Computers & Mathematics with Applications*. 2019;78(6):1960–1977. Available from: https://doi.org/10.1016/j.camwa.2019.03.033.
35) Shao WZ, Lin YZ, Liu YY, Wang LQ, Ge Q, Bao BK, et al. Gradient-based discriminative modeling for blind image deblurring. *Neurocomputing*. 2020;413:305–327. Available from: https://dx.doi.org/10.1016/j.neucom.2020.06.093.
36) Qi Q, Guo J, Jin W. EGAN: Non-uniform image deblurring based on edge adversarial mechanism and partial weight sharing network. *Signal Processing: Image Communication*. 2020;88(115952). Available from: https://dx.doi.org/10.1016/j.image.2020.115952.
37) Koh J, Lee J, Yoon S. Single-image deblurring with neural networks: A comparative survey. *Computer Vision and Image Understanding*. 2021;203:1–19. Available from: https://dx.doi.org/10.1016/j.cviu.2020.103134.
38) Zhang D, Liang Z, Shao J. Joint image deblurring and super-resolution with attention dual supervised network. *Neurocomputing*. 2020;412:187–196. Available from: https://dx.doi.org/10.1016/j.neucom.2020.05.069.
39) Zhang Y, Li W, Li Z, Ning T. Dual attention per-pixel filter network for spatially varying image deblurring. *Digital Signal Processing*. 2021;113:1–22. Available from: https://dx.doi.org/10.1016/j.dsp.2021.103008.
40) Chen X, Liu D, Zhang Y, Liu X, Xu Y, Shi C. Robust motion blur kernel parameter estimation for star image deblurring. *Optik*. 2021;230:1–23. Available from: https://dx.doi.org/10.1016/j.ijleo.2021.166288.
41) Zhang Y, Shi Y, Ma L, Wu J, Wang L, Hong H. Blind natural image deblurring with edge preservation based on L0-regularized gradient prior. *Optik*. 2021;225:165735–165735. Available from: https://dx.doi.org/10.1016/j.ijleo.2020.165735. doi:10.1016/j.ijleo.2020.165735.
42) Peng J, Shao Y, Sang N, Gao C. Joint image deblurring and matching with feature-based sparse representation prior. *Pattern Recognition*. 2020;103:1–23. Available from: https://dx.doi.org/10.1016/j.patcog.2020.107300.
43) Mallikarjunaswamy S, Sharmila N, Maheshkumar D, Komala M, Mahendra HN. Implementation of an effective hybrid model for islanded microgrid energy management. *Indian Journal of Science and Technology*. 2020;13(27):2733–2746. Available from: https://dx.doi.org/10.17485/ijst/v13i27.982.
44) Sree PH, Rao KS, and. A Novel Approach for Blurred Face Recognition System Using GLDA Features with LCDR Classification. *Indian Journal of Science and Technology*. 2019;12(29):1–8. Available from: https://dx.doi.org/10.17485/ijst/2019/v12i29/146975.
45) Liu J, Ma R, Zeng X, Liu W, Wang M, Chen H. An efficient non-convex total variation approach for image deblurring and denoising. *Applied Mathematics and Computation*. 2021;397:1–19. Available from: https://dx.doi.org/10.1016/j.amc.2021.125977.
46) Xu N. Adaptively Sparse Regularization for Blind Image Restoration. *Electrical Engineering and Systems Science*. 2021.